LETTERS

Eocene/Oligocene ocean de-acidification linked to Antarctic glaciation by sea-level fall

Agostino Merico[1,2], Toby Tyrrell[1] & Paul A. Wilson[1]

One of the most dramatic perturbations to the Earth system during the past 100 million years was the rapid onset of Antarctic glaciation near the Eocene/Oligocene epoch boundary[1–3] (~34 million years ago). This climate transition was accompanied[3] by a deepening of the calcite compensation depth—the ocean depth at which the rate of calcium carbonate input from surface waters equals the rate of dissolution. Changes in the global carbon cycle[4], rather than changes in continental configuration[5], have recently been proposed as the most likely root cause of Antarctic glaciation, but the mechanism linking glaciation to the deepening of calcite compensation depth remains unclear. Here we use a global biogeochemical box model to test competing hypotheses put forward to explain the Eocene/Oligocene transition. We find that, of the candidate hypotheses, only shelf to deep sea carbonate partitioning is capable of explaining the observed changes in both carbon isotope composition and calcium carbonate accumulation at the sea floor. In our simulations, glacioeustatic sea-level fall associated with the growth of Antarctic ice sheets permanently reduces global calcium carbonate accumulation on the continental shelves, leading to an increase in pelagic burial via permanent deepening of the calcite compensation depth. At the same time, fresh limestones are exposed to erosion, thus temporarily increasing global river inputs of dissolved carbonate and increasing seawater $\delta^{13}C$. Our work sheds new light on the mechanisms linking glaciation and ocean acidity change across arguably the most important climate transition of the Cenozoic era.

Evidence for Eocene ice rafting is compelling[6] but, despite speculation to the contrary[7], high-resolution oxygen isotope records[3,8] suggest that Cenozoic ice sheets approaching their modern size were not initiated on Antarctica until the Eocene/Oligocene boundary. Explanations for Antarctic glaciation at the Eocene/Oligocene boundary fall into two main categories: those invoking changes in ocean circulation through tectonic opening of Southern Ocean gateways, and those invoking changes in the global carbon cycle, with recent studies supporting the latter[4,9]. Proxy records of atmospheric CO_2 over the past 50 million years (Myr)[10] suggest an overall shift from high levels during the Eocene (~1,000 to ~2,000 parts per million by volume, p.p.m.v.) to lower levels thereafter. Support for a fall in CO_2 levels at the Eocene/Oligocene boundary comes from recent Ocean Drilling Program records[3]. These data show that deepening of the calcite compensation depth (CCD) across the Eocene/Oligocene boundary was rapid and took place in two jumps, in lockstep with the growth of Antarctic ice-sheets and carbon cycle perturbation—as tracked by changes in benthic foraminiferal calcite $\delta^{18}O$ and $\delta^{13}C$, respectively. Yet the mechanism teleconnecting the onset of major Antarctic glaciation and CCD deepening is a subject of debate. At least four hypotheses have been invoked to link $\delta^{18}O$ increase (glaciation), $\delta^{13}C$ increase and CCD deepening (carbon cycle perturbation) across this key interval. These are H1, an increase in organic carbon burial rates[2,11–13]; H2, an increase in weathering of silicate rocks[13–15]; H3, an increase in global siliceous (versus calcareous) plankton export production[3]; and H4, a shift of global $CaCO_3$ sedimentation from shelf to deep ocean basins[3,16,17].

To test the power of these hypotheses to explain the Eocene/Oligocene transition, we have developed a biogeochemical box model of the global ocean (Fig. 1) with long-term control on the carbon cycle given by weathering processes[18]. A full suite of time series are output, including nutrient and phytoplankton concentrations, alkalinity, dissolved inorganic carbon (DIC), pH, $[CO_3^{2-}]$ for sea water, CCD, $\delta^{13}C$ of burial fluxes plus atmospheric CO_2. In Fig. 2 we present the parameters best compared to the high-resolution data sets available: simulated CCD and $\delta^{13}C$ in benthic foraminiferal calcite.

In some ways H1 represents the obverse scenario to present-day fossil fuel emissions—a period of rapid burial of organic carbon (carbon sequestration) leading to CO_2 extraction from the atmosphere–ocean system. Eocene/Oligocene boundary sections in the Southern Ocean[11,19] show increased accumulation rates of opal and benthic foraminifera suggesting that elevated marine organic carbon burial rates contributed to ice-sheet growth via acceleration of the biological pump and CO_2 removal[2,11]. Higher pH associated with CO_2 drawdown would have increased $[CO_3^{2-}]$ and deepened the CCD.

At least three different processes have been proposed to elevate organic carbon burial at the Eocene/Oligocene boundary. Arguably the simplest (H1a) is increased nutrient supply via more vigorous stirring in a cooler climate with a steeper meridional temperature gradient and a large Antarctic ice sheet[5,13,20]. We test H1a by a permanent 3.5-fold increase in vertical mixing rates in the model (mixing between surface and middle boxes, and between middle and deep boxes, KSM and KMD, respectively, in Fig. 1). The simulation fails (Fig. 2a and b, red lines) to reproduce the proxy records by predicting a permanent change in benthic $\delta^{13}C$ and only a temporary change in the CCD (opposite to the observations). The latter reflects rapid depletion of the finite ocean nutrient inventory. The increase in ventilation also produces a pronounced temporary increase (by about 400 p.p.m.v.) in atmospheric p_{CO_2} (Supplementary Fig. 1)—at odds with the onset of Antarctic glaciation.

A second process (H1b) is increased efficiency of organic carbon burial at the sea floor[2], perhaps attributable to slower bacterial activity in a cooler climate[12]. We test H1b by employing a permanent 50% increase in the fraction of surface-produced organic carbon (and phosphorus) that survives to be buried. The simulation fails (Fig. 2a and b, green lines) by predicting a permanent change in $\delta^{13}C$, whereas observations show a recovery. Using a temporary version of the same perturbation fails by predicting a temporary change in both $\delta^{13}C$ and CCD.

[1]National Oceanography Centre, Southampton, European Way, Southampton SO14 3ZH, UK. [2]GKSS-Forschungszentrum, Institute for Coastal Research, Max Planck Straße 1, 21502, Geesthacht, Germany.

We test a third process (H1c) for increased organic carbon burial (increased nutrient delivery to the oceans) by supplying an additional 20% of both phosphorus and silicate down rivers. In these runs we decouple the effect of this perturbation from the weathering feedback by delivering the extra silicate through some (unspecified) process that does not simultaneously deliver alkalinity to the ocean. These simulations produce a modest increase in $\delta^{13}C$ followed by a persistent decline, and a CCD change that is of the wrong sign (Fig. 2a and b, black lines). CCD shoaling in these runs is traceable to calcifiers that are also being stimulated by the influx of extra nutrients, hence leading to a mismatch between carbonate burial and delivery down rivers.

The second hypothesis (H2) tested is that early Oligocene glaciation cycles enhanced silicate weathering[13–15], reducing atmospheric CO_2. Weathering of silicate rocks is a sink for atmospheric CO_2 and a source of alkalinity to the oceans and so, potentially, might explain both climate cooling and CCD deepening. A natural additional consequence of increased silicate weathering on the continents is elevated riverine delivery of silicate leading to increased oceanic diatom production (see H3). However, to isolate the direct impact of silicate weathering on the carbon cycle, under H2, we allow silicate weathering to affect ocean alkalinity but not silicate levels. Under this hypothesis, a strong decrease in carbonate weathering, driven by climate cooling, causes $[CO_3^{2-}]$ to fall sharply, with a consequent shallowing of the CCD (Fig. 2d). Sensitivity analyses using different injections of alkalinity, and different dependences of the two weathering processes on p_{CO_2} (Supplementary Fig. 6) produced the same conclusion (rejection of H2).

The increase in opal accumulation rates across the Eocene/Oligocene transition in the Southern Ocean[11,19] has also led to a third hypothesis (H3) in which the global balance shifted away from calcifiers towards silicifiers[3]. A plausible consequence of increased diatom dominance of phytoplankton assemblages is decreased abundance of other phytoplankton, including coccolithophores, because total production is limited by phosphate[21]. Assuming constant phosphorus and carbon river inputs, decreased surface production of $CaCO_3$ will eventually lead to an increase in $[CO_3^{2-}]$ and to a deepening of the CCD. In contrast to H2, we test this hypothesis by applying a permanent increase in the silicate riverine input to favour silicifiers against calcifiers. To decouple this perturbation from the weathering feedback, the extra silicate is delivered to the ocean through some (unspecified) process that does not simultaneously deliver alkalinity. The model captures some basic structure seen in the proxy records (for example, a permanent deepening of the CCD), but $\delta^{13}C$ does not recover to pre-excursion levels (Fig. 2e and f, red lines) when the perturbation is applied permanently. Applying the mechanism as a temporary perturbation results in a different mismatch with the data (simulated CCD shows only a temporary shift). An additional simulation in which increased silicate weathering is allowed to affect both alkalinity and silicate simultaneously (H2 in conjunction with H3) also produces unrealistic results with the effects of H2 outweighing those of H3.

A further hypothesis (H4) is a shift in the balance of global $CaCO_3$ burial from shelf to deep sea[3,16,17]. This hypothesis has two components[3]: glacioeustatic sea level fall[22] (by ~70 m) both reduces global shelf area and hence shelf burial of $CaCO_3$, and also exposes previously submarine shelf $CaCO_3$ to weathering. Modelling of the first component consists of a permanent decrease in shallow $CaCO_3$ burial. The second component, which has a temporary effect, consists of eroding and discharging to the ocean the newly exposed relatively fast-weathering[23] limestones. This extra discharge (~0.04–0.25 × 10^6 Gt $CaCO_3$-C in total; peak annual flux increased by ~50% to 300% over baseline, depending on the $\delta^{13}C$ of this carbonate) compares to an estimated[23,24] ~20% to 50% increase in global carbonate weathering during the Last Glacial Maximum (LGM) over today. Intense $CaCO_3$ erosion at the Eocene/Oligocene boundary is

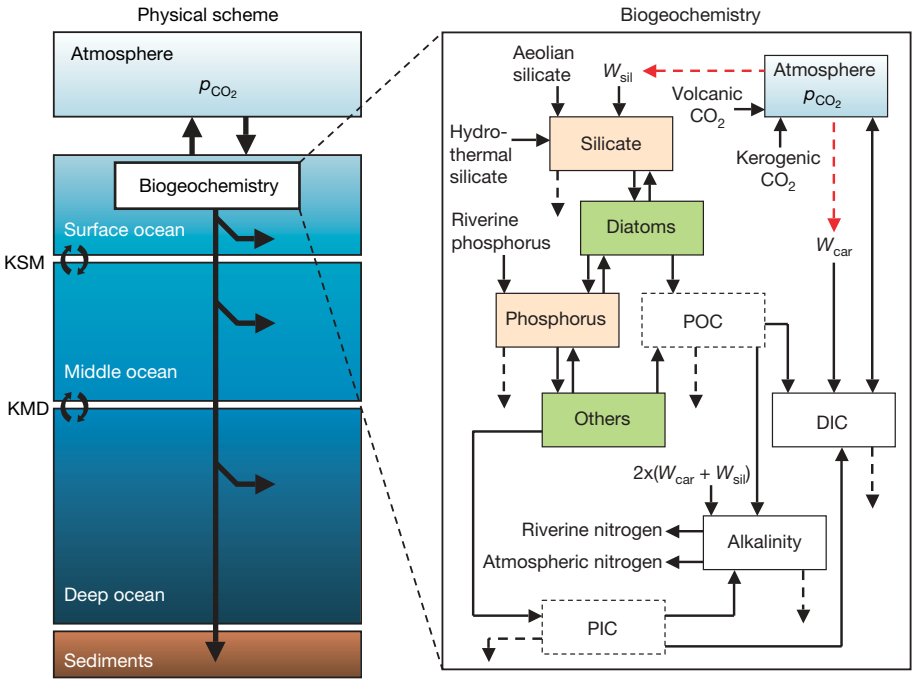

Figure 1 | Our global biogeochemical box model. The model comprises a three-box ocean module with an implicit sediment layer and an atmospheric box. The biology is modelled explicitly and includes diatoms and others (some of which represents calcifying phytoplankton), phosphorus and silicate. The distribution of DIC within the ocean is governed by physical, chemical and biological processes: the exchange of CO_2 between the atmosphere and the ocean, vertical advection of water, the organic carbon and calcium carbonate pumps and chemical speciation. Two of the processes reducing alkalinity are deposition of atmospheric nitrogen, and input of riverine nitrogen. In the biogeochemistry scheme, the dashed black arrows represent export out from the surface ocean. The silicate and carbonate feedbacks are indicated with dashed red arrows. PIC, particulate inorganic carbon; POC, particulate organic carbon; W_{car}, carbonate weathering; W_{sil}, silicate weathering; KSM and KMD, mixing between surface and middle boxes and between middle and deep boxes, respectively. The arrows in the oceanic boxes and sediments represent the various remineralization and sedimentation fluxes. A full list of variables and parameter values is given in Supplementary Tables 1 and 2.

based on a threefold greater Eocene inventory of shelf carbonate than today[17], and its likely much greater average solubility—having not undergone mineralogical stabilization during repeated precursor large-amplitude glacial lowstands. We model the Eocene/Oligocene input as a two-step function (Supplementary Fig. 3), in line with interpretations[3,4] of how the Antarctic ice sheet grew, but our findings are not sensitive to this implementation. In our 'best run', the CCD shows an overall permanent deepening with a maximum initial response of about 2 km; and $\delta^{13}C$ shows a temporary increase in agreement with the data (Fig. 2g and h, red lines).

We ascribe more importance to the similarity in form of the observed and modelled records than to absolute values for two reasons. First, the model captures the global signal, whereas the records come from a single site (albeit from the largest ocean). Second, the model is conservative in that Eocene global shelf-to-basin $CaCO_3$ partitioning is set to 45:55, close to the estimated present-day ratio[25], whereas the early Cenozoic shelf $CaCO_3$ sink was proportionately larger[17]. Accordingly, we conclude that H4 is compatible with the observations. A permanent shift in the CCD, towards deeper values, is induced by the requirement of the ocean to maintain the input/output balance of carbonate by a shelf-to-deep-basin switch in deposition. A change in $\delta^{13}C$ of the right sign and approximate magnitude is brought about by the weathering of extra neritic $CaCO_3$, having[26] a higher isotopic composition than the baseline $CaCO_3$ weathering and burial fluxes, both of which have substantial pelagic components (Supplementary Fig. 3).

It has been suggested[27] that increased weathering to the ocean of calcium ions is the critical process, via its effect on saturation state and the CCD. We test this alternative by re-running H4, but with $[Ca^{2+}]$ as a dynamic variable rather than a constant. In this experiment all $CaCO_3$ fluxes affect $[Ca^{2+}]$ as well as DIC and alkalinity. Given the large difference in residence times (calcium ~1 million years; DIC ~100,000 years) and concentrations (calcium ~10.6 mmol; DIC ~2.3 mmol), the addition of calcium produces a negligible difference to the model results (the green lines in Fig. 2g and h almost directly overlie their red line counterparts). We therefore discount this alternative.

The $\delta^{13}C$ and $CaCO_3$ MAR records from ODP Site 1218 provide strong constraints on the biogeochemistry of Eocene/Oligocene

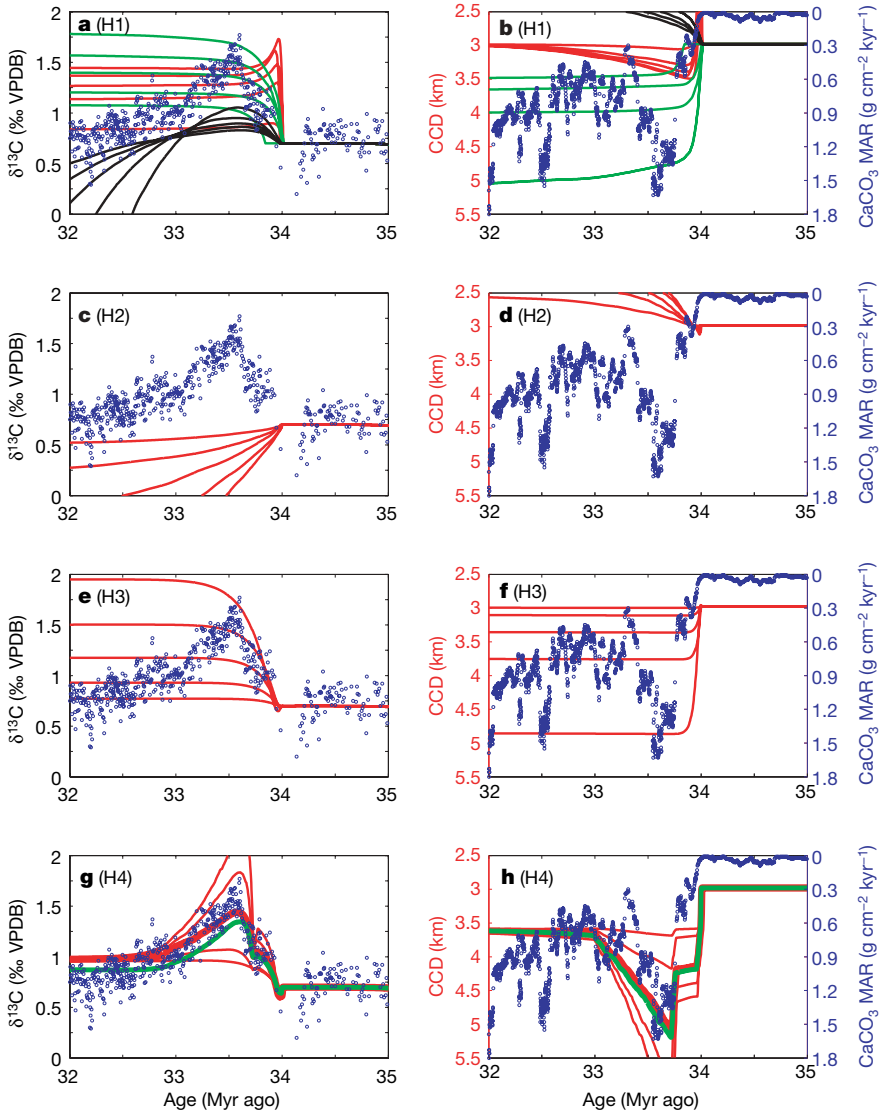

Figure 2 | Model results simulating competing hypotheses and comparison to available data. Carbon isotope ratios in benthic foraminifera (**a**, **c**, **e** and **g**) and CCD evolution (**b**, **d**, **f** and **h**) for families of runs simulating the four different hypotheses H1, H2, H3 and H4 compared to the data[3]. **a**, **b**, H1 shows increased organic carbon burial via: a more vigorous stirring of the ocean (red lines), increased efficiency of organic carbon burial at the sea floor (green lines), and increased nutrient delivery to the ocean (black lines). **c**, **d**, H2 shows enhanced weathering of silicate rocks (red lines). **e**, **f**, H3 shows silicifiers outcompeting calcifiers (red lines). **g**, **h**, H4 shows changes in shelf to deep basin $CaCO_3$ partitioning and erosion of newly exposed $CaCO_3$ as a result of sea-level fall, affecting the seawater saturation state via dumping of additional carbon to the ocean (red lines; we consider the thick red line to be our 'best run'), and via dumping of both carbon and calcium in a 1:1 ratio (green line). Extra calcium was added only to the 'best run'.

boundary events: a temporary increase in $\delta^{13}C$ followed by a full recovery, and a large deepening in the CCD, followed by only partial recovery such that a permanent deepening in the CCD of order 1 km is sustained. Any hypothesis must simultaneously account for both the permanent and the temporary changes. Only H4 is found to do this, when applied to our model.

Glacioeustatic sea-level fall associated with the growth of the Antarctic ice sheet exposes widespread limestones to erosion; this leads to a one-off 'dump' of dissolved inorganic carbon and alkalinity into the ocean, increasing $[CO_3^{2-}]$, deepening the CCD and increasing seawater $\delta^{13}C$. The reduction in shelf habitat for neritic benthic calcifiers leads to a large reduction in $CaCO_3$ burial state in shallow seas, with superimposed shorter term fluctuations as the East Antarctic ice sheet varies in size in response to orbital forcing[3,28]. Because river inputs of dissolved $CaCO_3$ must match global $CaCO_3$ burial[29], the decline in shallow-sea burial forces a compensating increase in deep-sea burial through a shift in state to a deeper CCD.

In nature, we might expect shelf to basin $CaCO_3$ fractionation to act in concert with other processes but additional runs to test H4 in combination with H1, H2 and H3 each resulted in poorer simulations of the high-resolution data sets available (Supplementary Fig. 2). Improved p_{CO_2} records are needed. Our simulations show that, acting alone, H4 brings about a large but transient p_{CO_2} decline (Supplementary Fig. 1). If CCD deepening at the Eocene/Oligocene boundary marks a permanent shift to a lower p_{CO_2} regime then additional processes are indicated. Either way, our findings in support of a sea-level-led hypothesis (H4) lend weight to the view[3] that rapid carbon-cycle perturbation associated with CCD deepening at the Eocene/Oligocene boundary did not trigger Antarctic glaciation. Instead, rapid glaciation, itself driven by slow long-term CO_2 drawdown via silicate weathering[4] and orbital forcing[3] (inhibiting warm Antarctic summers), is capable of triggering a chain of carbon cycle responses, including CCD deepening, $\delta^{13}C$ perturbation and associated further (ice-sheet-stabilizing) rapid p_{CO_2} drawdown, cooling and aridification[30].

METHODS SUMMARY

Our biogeochemical box model of the global ocean includes two phytoplankton groups: diatoms and others (the latter including calcifiers) and the cycling of silicate, phosphorus, DIC and alkalinity (Fig. 1). The model simulates dynamic changes in the CCD and ocean carbon chemistry is linked, through air–sea gas exchange, with atmospheric CO_2. Both ^{12}C and ^{13}C are simulated in each reservoir and flux. Long-term control on the carbon cycle is given by weathering processes[18]. A full list of variables and parameter values is given in Supplementary Tables 1 and 2.

Full Methods and any associated references are available in the online version of the paper at www.nature.com/nature.

Received 21 September 2007; accepted 19 February 2008.

1. Miller, K. G., Wright, J. D. & Fairbanks, R. G. Unlocking the icehouse: Oligocene-Miocene oxygen isotopes, eustasy, and margin erosion. *J. Geophys. Res.* **96,** 6829–6849 (1991).
2. Zachos, J. C., Quinn, T. M. & Salamy, K. A. High-resolution (10^4 years) deep-sea foraminiferal stable isotope records of the Eocene-Oligocene climate transition. *Palaeoceanography* **11,** 251–266 (1996).
3. Coxall, H. K., Wilson, P. A., Pälike, H., Lear, C. H. & Backman, J. Rapid stepwise onset of Antarctic glaciation and deeper calcite compensation in the Pacific Ocean. *Nature* **433,** 53–57 (2005).
4. DeConto, R. M. & Pollard, D. Rapid Cenozoic glaciation of Antarctica triggered by declining atmospheric CO_2. *Nature* **421,** 245–249 (2003).
5. Kennett, J. P. & Shackleton, N. J. Oxygen isotopic evidence for the development of the psychrosphere 38 Myr ago. *Nature* **260,** 513–515 (1976).
6. Eldrett, J. S., Harding, I. C., Wilson, P. A., Butler, E. & Roberts, A. P. Continental ice in Greenland during the Eocene and Oligocene. *Nature* **446,** 176–179 (2007).
7. Tripati, A., Backman, J., Elderfield, H. & Ferretti, P. Eocene bipolar glaciation associated with global carbon cycle changes. *Nature* **436,** 341–346 (2005).
8. Edgar, K. M., Wilson, P. A., Sexton, P. S. & Suganuma, Y. No extreme bipolar glaciation during the main Eocene calcite compensation shift. *Nature* **448,** 908–911 (2007).
9. Lyle, M., Gibbs, S., Moore, T. C. & Rea, D. K. Late Oligocene initiation of the Antarctic Circumpolar Current: Evidence from the South Pacific. *Geology* **35,** 691–694 (2007).
10. Pagani, M., Zachos, J. C., Freeman, K. H., Tipple, B. & Bohaty, S. Marked decline in atmospheric carbon dioxide concentrations during the Paleogene. *Science* **309,** 600–603 (2005).
11. Salamy, K. A. & Zachos, J. C. Latest Eocene-Early Oligocene climate change and Southern Ocean fertility: inferences from sediment accumulation and stable isotope data. *Palaeogeogr. Palaeoclimatol. Palaeoecol.* **145,** 61–77 (1999).
12. Olivarez Lyle, A. & Lyle, M. W. Missing organic carbon in Eocene marine sediments: is metabolism the biological feedback that maintains end-member climates? *Paleoceanography* **21,** PA2007, doi:10.1029/2005PA001230 (2006).
13. Zachos, J. C. & Kump, L. R. Carbon cycle feedbacks and the initiation of Antarctic glaciation in the earliest Oligocene. *Glob. Planet. Changes* **47,** 51–66 (2005).
14. Zachos, J. C., Opdyke, B. N., Quinn, T. M., Jones, C. E. & Hallid, A. N. Early cenozoic glaciation, Antarctic weathering, and seawater $^{87}Sr/^{86}Sr$: is there a link? *Chem. Geol.* **161,** 165–180 (1999).
15. Ravizza, G. E. & Peucker-Ehrenbrinck, F. The marine $^{187}Os/^{188}Os$ record of the Eocene-Oligocene transition: the interplay of weathering and glaciation. *Earth Planet. Sci. Lett.* **210,** 151–165 (2003).
16. Kump, L. R. & Arthur, M. A. in *Tectonic Uplift and Climate Change* (ed. Ruddiman, W. F.) 399–426 (Plenum, New York, 1997).
17. Opdyke, B. N. & Wilkinson, B. H. Surface area control of shallow cratonic to deep marine carbonate accumulation. *Paleoceanography* **3,** 685–703 (1988).
18. Walker, J. C. G. & Kasting, J. F. Effects of fuel and forest conservation on future levels of atmospheric carbon dioxide. *Palaeogeogr. Palaeoclimatol. Palaeoecol.* **97,** 151–189 (1992).
19. Diester-Haass, L. Middle Eocene to early Oligocene paleoceanography of the Antarctic Ocean (Maud Rise, ODP Leg 113, Site 689): change from a low to a high productivity ocean. *Palaeogeogr. Palaeoclimatol. Palaeoecol.* **113,** 311–334 (1995).
20. Kennett, J. P. Cenozoic evolution of Antarctic glaciation, the circum-Antarctic Ocean, and their impact on global paleoclimate. *J. Geophys. Res.* **82,** 3843–3860 (1977).
21. Tyrrell, T. The relative influence of nitrogen and phosphorus on oceanic primary prduction. *Nature* **400,** 525–531 (1999).
22. Pekar, S. F., Christie-Blick, N., Kominz, M. A. & Miller, K. G. Calibration between eustatic estimates from backstripping and oxygen isotopic records for the Oligocene. *Geology* **30,** 903–906 (2002).
23. Gibbs, M. T. & Kump, L. R. Global chemical erosion during the last glacial maximum and the present: sensitivity to changes in lithology and hydrology. *Paleoceanography* **9,** 529–543 (1994).
24. Munhoven, G. Glacial-intergalacial changes of continental weathering: estimates of the related CO_2 and HCO_3- flux variations and their uncertainties. *Glob. Planet. Changes* **33,** 155–176 (2002).
25. Milliman, J. D. Production and accumulation of calcium carbonate in the ocean: budget of a nonsteady state. *Glob. Biogeochem. Cycles* **7,** 927–957 (1993).
26. Swart, P. K. & Eberli, G. The nature of $\delta^{13}C$ of periplatform sediments: Implications for stratigraphy and the global carbon cycle. *Sedim. Geol.* **175,** 115–129 (2005).
27. Rea, D. K. & Lyle, M. W. Paleogene calcite compensation depth in the eastern subtropical Pacific: answers and questions. *Paleoceanography* **20,** PA1012, doi:10.1029/2004PA001064 (2005).
28. Pälike, H. *et al.* The heartbeat of the Oligocene climate system. *Science* **314,** 1894–1898 (2006).
29. Zeebe, R. & Westbroek, P. A simple model for the CaCO3 saturation state of the ocean: The "Strangelove", the "Neritan", and the "Cretan" ocean. *Geochem. Geophys. Geosyst.* **4,** doi:10.1029/2003GC000538 (2003).
30. Dupont-Nivet, G. *et al.* Tibetan plateau aridification linked to global cooling at the Eocene–Oligocene transition. *Nature* **445,** 635–638 (2007).

Supplementary Information is linked to the online version of the paper at www.nature.com/nature.

Acknowledgements We thank P. Sexton for discussions. We gratefully acknowledge R. DeConto, J. Kasting, G. Munhoven, H. Pälike and J. Walker for their comments on various aspects of our model, K. Wirtz for support and the UK Natural Environment Research Council for funding. We also thank R. Zeebe for comments on the manuscript.

Author Contributions All three authors contributed equally to this work.

Author Information Reprints and permissions information is available at www.nature.com/reprints. Correspondence and requests for materials should be addressed to A.M. (agostino.merico@gkss.de).

METHODS

Description of the model. The ocean component, developed from previous work[18,31], includes three vertically stacked boxes: the surface (0–100 m), which represents the euphotic zone, a middle box (100–500 m), which represents the mixed surface layer above the annual thermocline, and a deep box (500–3,730 m), which represents the deep layer below the annual thermocline. The model represents an average water column down to the seabed, has a spatially and temporally averaged input of nutrients, DIC and alkalinity, and does not take into account any latitudinal or horizontal variations. The distribution of DIC within the ocean is governed by physical, chemical and biological processes: the exchange of CO_2 between the atmosphere and the ocean, riverine input of DIC, biological uptake of CO_2 into biomass, remineralization and burial of biomass, precipitation and dissolution of $CaCO_3$ and mixing processes between the three layers. The processes governing the distribution of alkalinity in the ocean are: riverine input of bicarbonate and nitrate, precipitation of $CaCO_3$ by organisms and the biological uptake of nitrate, the dissolution of $CaCO_3$ deeper in the ocean and the remineralization of nitrate, burial of $CaCO_3$ and mixing processes between the three layers. The production of $CaCO_3$ in the surface ocean is linked to the production of organic matter through the 'rain ratio', which is the molar ratio of particulate inorganic carbon (PIC) export from the surface layer to particulate organic carbon (POC) export.

The silicate and carbonate weathering processes are modelled (according to ref. 18) using: $W_{car} = f_{car} \times (p_{CO_2} / p_{CO_{2(ini)}})$ and $W_{sil} = f_{sil} \times (p_{CO_2} / p_{CO_{2(ini)}})^{0.3}$. W_{car} and W_{sil} are normalized to the initial p_{CO_2} value: $p_{CO_2(ini)}$. Input terms to the atmosphere also include a weathering process, the oxidation of fossil POC from rocks (kerogenic input), as well as CO_2 from volcanic outgassing (volcanic input).

The model includes the calculation of the dynamic CCD and aragonite compensation depth (ACD). Ocean hypsometry was obtained from the ETOPO5 data set at 5×5 min resolution across the global ocean. The relative fractions of ocean area at different depths were calculated by summing over the data set. To prevent unrepresentative biasing towards polar latitudes, each grid cell was weighted by the cosine of its latitude. The critical carbonate ion concentration ($[CO_3^{2-}]_{crit}$) below which sea water is undersaturated is a function of depth and is dependent on the crystal structure, specifically, calcite (mainly foraminifera and coccolithophores) or aragonite (mainly neritic calcifiers). The model calculates deep carbonate ion concentration, and the following equations[32] (for calcite and aragonite respectively) $[CO_3^{2-}]_{crit}(z) = 88.7\exp[0.189(z-3.82)]$ and $[CO_3^{2-}]_{crit}(z) = 117.5\exp[0.176(z-3.06)]$ are used to calculate the depth at which $[CO_3^{2-}]_{crit} = [CO_3^{2-}]$. The ocean hypsometry is then used to calculate the fraction of ocean area above or below the CCD and the ACD, and hence the proportions of the sinking $CaCO_3$ flux that are buried or dissolved.

The rate of $CaCO_3$ dissolution in the model is calculated solely as the product of the $CaCO_3$ sinking flux and the fraction of sea floor receptive to $CaCO_3$ burial. Previous carbon cycle studies[33–36] have included chemical erosion and/or respiration-driven dissolution. However, although chemical erosion of previously deposited $CaCO_3$ in the bioturbated zone must be considered for an ocean becoming increasingly acidic, it is not crucial for this study, in which the CCD is deepening. Respiratory dissolution does not generally decouple the lysocline from the saturation horizon[34] and so was not included. Following ref. 29, dissolution of $CaCO_3$ is modelled without explicitly modelling sediment chemistry.

Stable isotope composition of the shell calcite of most species of foraminifera reveals offsets from calcite precipitated in equilibrium with the ambient bottom water[37]. These offsets have been attributed to so-called vital effects. Evidence from culture experiments[38] suggests a significant effect of seawater carbonate ion concentration on the stable isotope composition of planktic foraminifera. This aspect was also taken into account in our model by using[38]: $\delta^{13}C_{shell} = \delta^{13}C_{DIC} - 0.008([CO_3^{2-}] - 300)$. We also include the CO_2 effect on the $\delta^{13}C$ of POC by using the following[39]: $\delta^{13}C_{org} = \delta^{13}C_{DIC} - 9866/T_K + 24.12 - 17\log_{10}([CO_{2(aq)}]) + 3.4$.

We note that whereas the model is based on a rather simple physical scheme of the global ocean (three vertical boxes), a previous study[4] (using a complex general circulation model with coupled components for atmosphere, ocean, ice sheet and sediment) has shown that physical processes (driven for instance by changes in continental configuration) had only a secondary role in the Eocene/Oligocene climate transition, compared to the processes controlling CO_2 concentration. A sensitivity analysis investigation suggests that the results obtained here are insensitive to model simplifications and assumptions (Supplementary Information).

Steady-state and implementation of perturbations. The initial time of the simulations is the late Eocene (35 Myr ago). The model is run for 3 Myr across the Eocene/Oligocene boundary up to the early Oligocene (32 Myr ago). We start the model in the steady state, then apply a perturbation in accordance with each hypothesis at the Eocene/Oligocene boundary. As part of the sensitivity analysis, we generated a family of runs for each hypothesis by changing parameter values. We choose to establish the initial steady state at an atmospheric p_{CO_2} of 1,000 p.p.m.v. ($p_{CO_2\ (ini)}$), in keeping with proxy records[10]. In accordance with the data available[3] from the Pacific ('global') ocean, this steady-state is characterized by $\delta^{13}C$ in benthic foraminifera of +0.7‰ VPDB (Vienna Pee-Dee Belemnite standard) and depths for the CCD and ACD of about 3 km and 0.7 km, respectively. Major fluxes resulting from this baseline steady state are reported in Supplementary Table 3.

31. Chuck, A., Tyrrell, T., Totterdell, I. J. & Holligan, P. M. The oceanic response to carbon emissions over the next century: investigation using three ocean carbon cycle models. *Tellus B* **57,** 70–86 (2005).
32. Jansen, H., Zeebe, R. E. & Wolf-Gladrow, D. A. Modeling the dissolution of settling $CaCO_3$ in the ocean. *Glob. Biogeochem. Cycles* **16,** doi:10.1029/2000GB001279 (2002).
33. Archer, D. A data-driven model of the calcite lysocline. *Glob. Biogeochem. Cycles* **10,** 511–526 (1996).
34. Sigman, D. M., McCorkle, D. C. & Martin, W. R. The calcite lysocline as a constraint on glacial/interglacial low-latitude production changes. *Glob. Biogeochem. Cycles* **12,** 409–427 (1998).
35. Broecker, W. S. & Peng, T.-H. The role of CaCO3 compensation in the glacial to interglacial atmospheric CO2 change. *Glob. Biogeochem. Cycles* **1,** 15–29 (1987).
36. Ridgwell, A. *et al.* Marine geochemical data assimilation in an efficient Earth System Model of global biogeochemical cycling. *Biogeosciences* **4,** 87–104 (2007).
37. Rohling, E. J. & Cooke, S. in *Modern Foraminifera* (ed. Sen Gupta, B. K.) 239–258 (Kluwer Academic, Dordrecht, 1999).
38. Spero, H. J., Bijma, J., Lea, D. W. & Bemis, B. E. Effect of seawater carbonate concentration on foraminiferal carbon and oxygen isotopes. *Nature* **390,** 497–500 (1997).
39. Hofmann, M., Broecker, W. S. & Lynch-Stieglitz, J. Influence of a $[CO_{2(aq)}]$ dependent biological C-isotope fractionation on glacial $^{13}C/^{12}C$ ratios in the ocean. *Glob. Biogeochem. Cycles* **13,** 873–883 (1999).